DOE-HEP Final Report for 2013-2016

08/08/2016

DE-SC0010012, Duke University

PI: Prof. Thomas Katsouleas
Personnel: Aakash Sahai (graduate student)

Funding period - 04/01/2013 to 03/31/2016

Stated Goals

1. Studies of plasma wakefields for high repetition-rate plasma collider
2. Theoretical study of laser-plasma proton and ion acceleration

Publications

Corresponding to Stated Goal # 1

1. Long-term evolution of plasma wakefields, **MOPAC10**, Proceedings of PAC 2013, Pasadena, CA, USA
2. Self-injection by trapping of plasma electrons oscillating in rising density gradient at the vacuum-plasma interface, **TUPME051**, Proceedings of IPAC 2014, June 2014, Dresden, Germany
3. Improving the Self-Guiding of an Ultraintense Laser by Tailoring Its Longitudinal Profile, Phys. Rev. Lett. 113, 245001, Dec 2014
4. Ion-wake excitation due to interaction with non-linear electron wakefields, [submitted / under review]
5. Optimal positron-beam excited plasma wakefields in hollow and ion-wake channels, **WEPJE001**, Proceedings of IPAC2015, Richmond, VA, USA

Corresponding to Stated Goal # 2

6. Longitudinal instabilities affecting the moving critical layer laser-plasma ion accelerators, Proceedings of Advanced Accelerators Concepts, July 2014
7. Motion of the plasma critical layer in plasma with immobile and mobile ions for ion acceleration applications, Phys. Plasmas **21**, 056707 (2014)

Stated goal # 1 – Studies of wakefields for high repetition rate plasma collider

Excitation of a Non-linear Ion-wake (10s of picosecond behind the energy-source driving the plasma wakefields) [1][4] – An analytical model was developed to determine the ion-motion resulting from the interaction of non-linear "blow-out" wakefields excited by beam-plasma and laser-plasma interactions. This is key to understanding the state of the plasma at timescales of 1 picosecond to a few 10s of picoseconds behind the driver-energy pulse.

The motion of ion-rings experiencing "focusing" and "de-focusing" radial forces from the electron wakefields was modeled. As the electron wakefields have nearly zero group velocity even though the oscillation phase velocity is nearly the group velocity of the driver in the plasma. Thus, there is an extended interaction between the electron wakefields excited in the wake of the driver and the background ions.

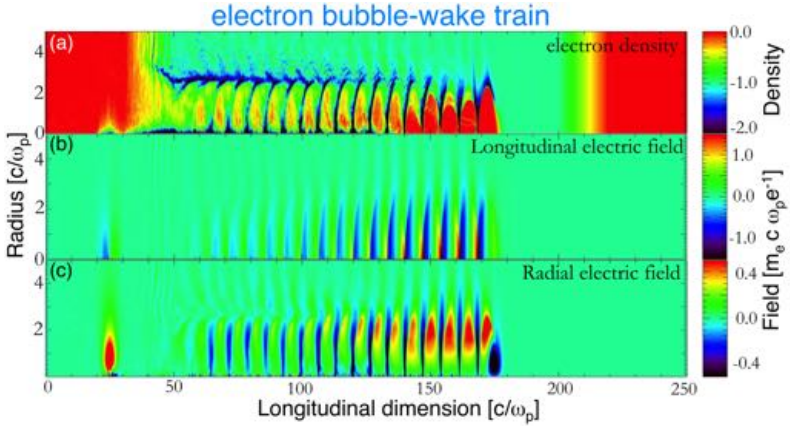

FIG. 3: **Longitudinally asymmetric phases and the time-evolution of a "bubble" and the bubble-train**. (a) electron beam-driven bubble-train electron density in 2D cylindrical real-space, (b) corresponding longitudinal electric field profile and (c) corresponding radial-field profile. The beam-plasma parameters are same as in Fig.2 but the electron-wake is shown at an earlier time.

With the help of analytical theory and simulations it was determined that the ions respond to 2 different "phases" of focusing forces of the oscillating electron plasma wakefields. During the oscillation of the plasma wakefields the regions where the back of the bubble has a large electron compression the radial fields are "de-focusing" for electrons but "focusing" for background ions, so the ions tend to move to the axis. Whereas in the region of the cavitation where only background ions exist the radial forces are "defocussing" for background ions.

$$m_i d^2 r_{ion}/dt^2 = \Sigma F_{ion} \qquad \frac{d^2 r}{dt^2} = F_{wake}^{back} + F_{wake}^{edge} + F_{ponde}^{laser} + F_{beam} + F_{sc}^{ion}$$

$$m_{ion} d^2 r_{ion}/dt^2 - \frac{v_\phi}{\lambda_{Np}}(F^{sc}\tau_{bubble} - F_e^{back}\tau_{back}) = 0$$

$$d^2 r_{ion}/dt^2 + \frac{v_\phi \tau_{bubble}}{\lambda_{Np}} \frac{\omega_{pi}^2}{2}\left(\frac{n_{be}}{n_0}\frac{\tau_{back}}{\tau_{bubble}}\frac{r_{be}^2}{r_{ion}^2} - 1\right) r_{ion} = 0$$

$$r_{ion}^{eq} = r_{be}\sqrt{\frac{n_{be}}{n_0}\frac{\tau_{back}}{\tau_{bubble}}}$$

From computational modeling of the extended interaction of the non-linear "blow-out" electron-wake with the background plasma we see the ion-wake excited in the form of a near-hollow channel. We simulate many different laser and plasma parameters to confirm the model of the excitation of an ion-wake.

We have shown that the ion-wake channel is an ion soliton of the type modeled with a cKdV equation. However, the conventional cKdV model does not entirely apply to our problem and thus our model significantly differs from cKdV equation.

Firstly, the electrons only develop a temperature in the plasma region where the electron-beam propagates and where the electron wakefields develop and eventually phase-mix away.

Secondly, in the cKdV model for an ion soliton, the plasma is assumed to be equilibrated and isothermal which is not the condition for a wake heated plasma.

Thirdly, it is well known that the cylindrical ion-soliton changes amplitude as it propagates, which is unlike a 1D soliton. The cylindrical soliton decays as it propagates outwards. However, in this case the soliton does not decay as it propagates outwards, this is due to the continuous driver term resulting from the temperature gradient within the soliton.

$$\Phi^{(1)} = n_e^{(1)} = v^{(1)} = n_i^{(1)} \equiv \mathcal{U}$$

$$\frac{\mathcal{U}}{\tau} + 2\frac{\partial}{\partial\tau}\mathcal{U} + 2\mathcal{U}\frac{\partial}{\partial\xi}\mathcal{U} + \frac{\partial^3}{\partial\xi^3}\mathcal{U} = -\mathcal{U}\frac{\partial}{\partial\xi}T_e^{(1)}$$

The forced-cKdV model predicts that due to the effect of the hot electrons within the soliton and temperature gradient (seen as the driver term in the equation), the ion-soliton sustains for a much longer duration and thus propagates for much longer radial distance.

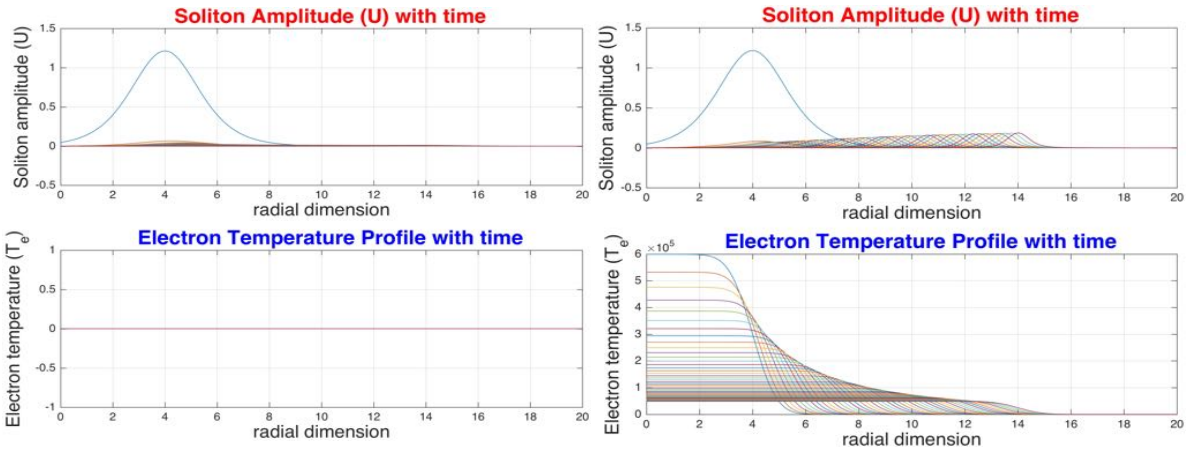

Figure 1 - Comparing the evolution of a cylindrical ion soliton by numerically solving the cKdV equation - when there is NO temperature gradient in CONTRAST to when there is

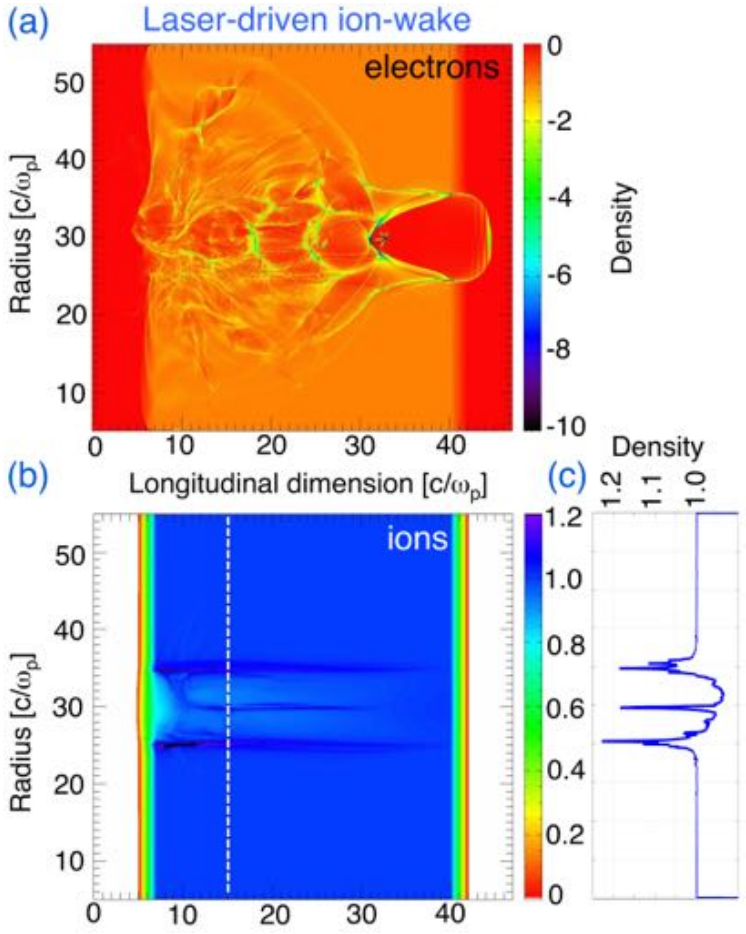

FIG. 1: **Laser driven non-linear ion-wake at 46ω_{pe}^{-1} in $m_i = m_p = 1836\, m_e$ plasma**. (a) electron bubble wakefields in cartesian coordinates (fixed-box) with $\frac{\omega_0}{\omega_{pe}} = 10$ driven by a matched laser pulse (vector potential $a_0 = 4$ and frequency ω_0) at time, t = 46 ω_{pe}^{-1} (0.17 f_{pi}^{-1}) with $R_B \simeq 4\frac{c}{\omega_{pe}}$. (b) non-linear ion-wake in the form of a cylindrical ion-soliton of radius $\simeq 4\frac{c}{\omega_{pe}}$ excited behind the bubble electron wake in a proton plasma. (c) transverse ion-density profile at $z = 150\, c/\omega_{pe}$. Notice that the ion density perturbation in this formation phase is still a fraction of the background ion density, $\frac{\delta n_i}{n_0} \ll 1$.

Figure 2 - Laser driven wakefield and formation of the channel (parameters in the figure), also shown is the lineout of the ion-channel density

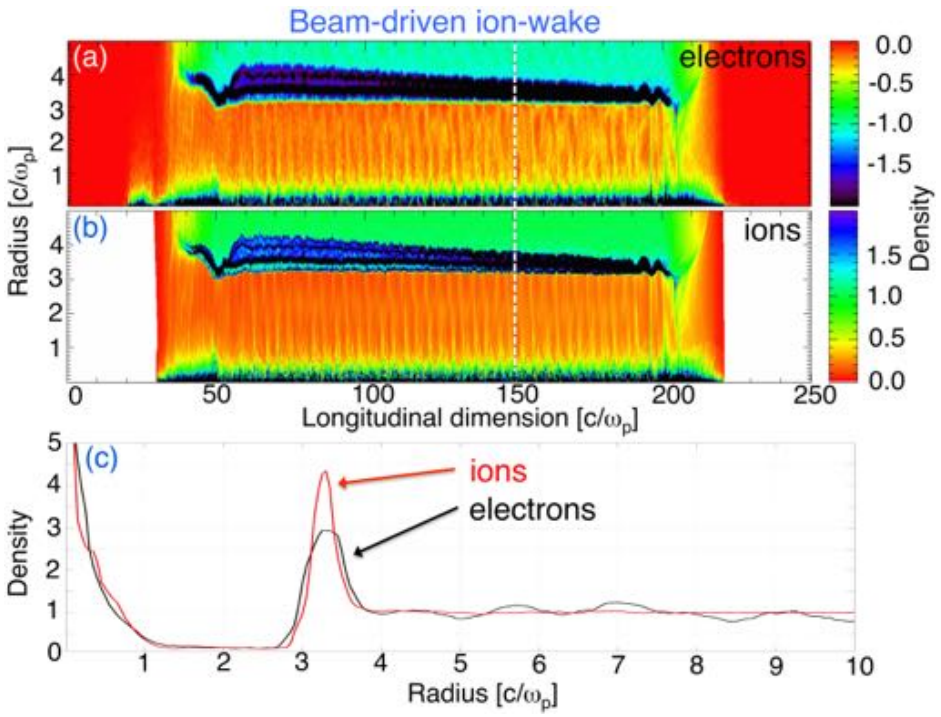

FIG. 2: **Electron beam-driven non-linear ion-wake at $460\omega_{pe}^{-1}$ in $m_i = m_p = 1836\, m_e$ plasma**. (a) Beam-driven ion-wake electron density in cylindrical coordinates (fixed-box) at time 460 ω_{pe}^{-1} (1.7 f_{pi}^{-1}). The beam parameters are $n_b = 5n_0$, $\sigma_r = 0.5c/\omega_{pe}$, $\sigma_z = 1.5c/\omega_{pe}$, $\gamma_b = 38,000$, these beam-plasma parameters are quite similar to [4]. (b) Corresponding ion density in cylindrical coordinates (fixed-box) at time 460 ω_{pe}^{-1}. It is quite interesting to note the N-soliton formation in the ion-density. This is seen as the ion-wake evolves further, for instance at $z = 60\, c/\omega_{pe}^{-1}$. (c) radial electron and ion density profile at $z = 150\, c/\omega_{pe}$.

Figure 3 - non-linear ion-wake of an electron-beam driven electron wake and the lineout of electron-ion density along the radial dimension at the marked longitudinal location

We have also modeled the expansion of the hollow-channel due to the electron temperature in the hollow region of the ion soliton. We've submitted the manuscript for consideration and are currently in the process of comparing it against experiments at SLAC.

Ion-channel Experiments at FACET using the SLAC electron beam at sector 20

- wakefield visualization efforts were carried out at SLAC national lab in collaboration with Prof Downer's team at UT-Austin as part of the experiment E-224.
Installation of the equipment and the first proof-of-principle experiments were setup with our active participation in the first quarter of 2014. Proof-of-principle data was gathered in second quarter of 2014. Several very interesting non-linear ion-wake results were obtained.

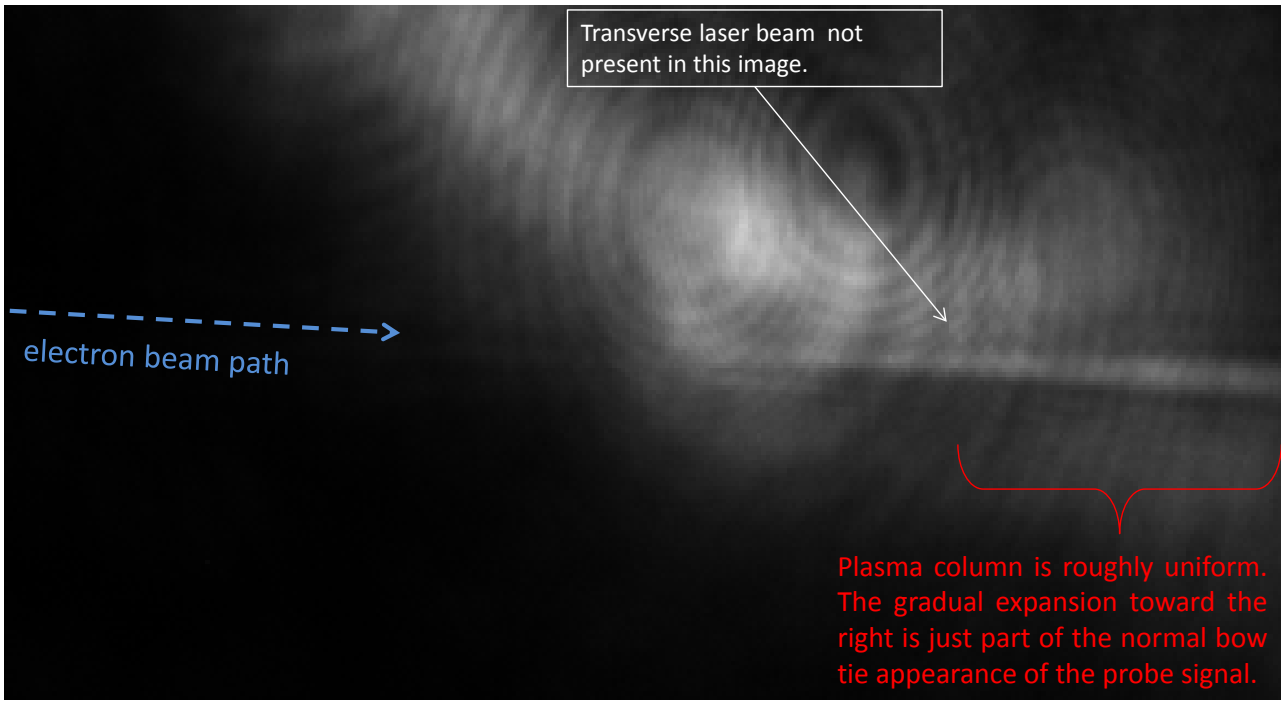

Figure 4 - Formation of the nonlinear ion-wake of electron-beam driven wakefields in the "bubble" regime

Positron acceleration in hollow and ion-wake (near-hollow) channels [5]

– We further explore the "suck-in" regime of positron beam in a hollow plasma channel under the non-linear interaction regime. We try to understand the possibility of using the ion-wake near-hollow channel plasma for positron acceleration, to be published [5].

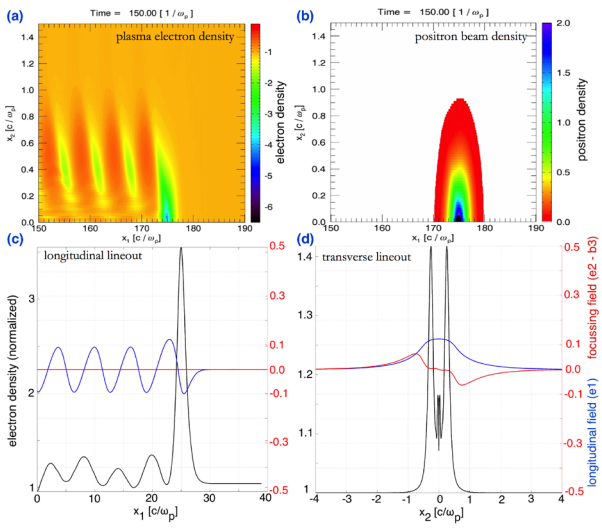

FIG. 1: **Positron-beam driven wakefields in a homogeneous plasma** (a) electron density in 2D cylindrical space at $t = 150\omega_{pe}^{-1}$ (b) positron-beam in 2D cylindrical space (c) on-axis longitudinal (x_1) line-out: electron density (black), longitudinal field (blue), focussing field (red) (d) transverse (x_2) line-out at the peak longitudinal field.

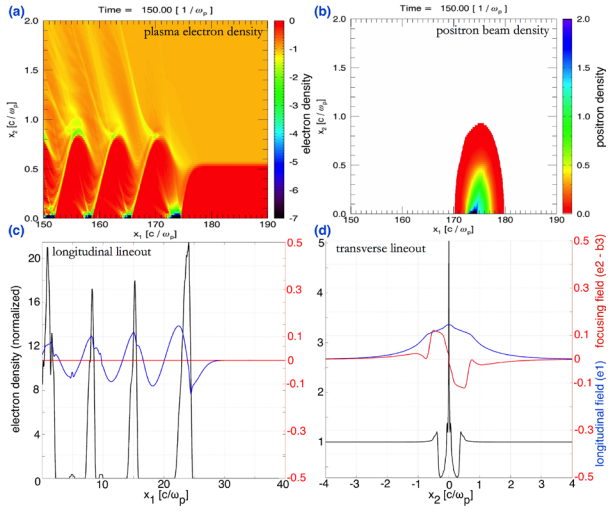

FIG. 2: **Positron-beam driven wakefields in a hollow-plasma channel with** $r_{ch} = 0.55\frac{c}{\omega_{pe}}$, with panels equivalent to Fig.1

Figure 5 - Positron acceleration comparison in homogeneous plasma compared to a perfectly matched Hollow-channel

Self-injection in a rising density gradient [2] – proposed a scheme of self-injection of plasma e- into the wakes due to phase-mixing of longitudinal oscillations in a rising plasma density gradient. Using an analytical model we study the scaling laws to determine if the trapping mechanism scales with the driver and plasma parameters per model predictions. Such density gradients are part of all plasma sources.

We are currently preparing a manuscript of this mechanism and intend to collaborate to expt-ly demonstrate it.

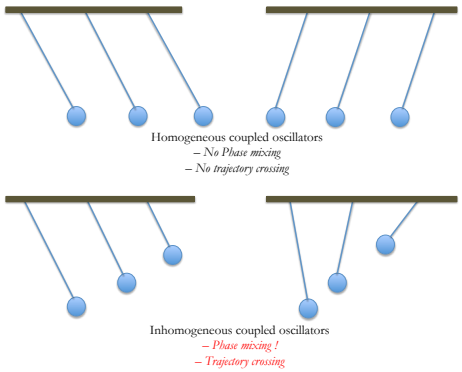

FIGURE 6.2: **Phase mixing of coupled oscillators with spatially increasing frequencies.** Individual plasmons excited in the wake of a driver in a homogeneous plasma are coupled together and undergo in-phase or synchronous-phase oscillations. However, in an inhomogeneous rising density plasma (common at the vacuum-plasma interface of plasma sources), the individual plasmons have increasing characteristic frequency. Hence there is phase-mixing and trajectory crossing.

$$\Delta t_{mix} = \frac{\pi}{2\frac{\partial \omega_{pe}(x)}{\partial x}\xi_m}$$

$$\left(\frac{1}{c^2}\frac{\partial^2}{\partial t^2} + k_{pe}^2\right)[\gamma\beta_\parallel] = -\frac{1}{c}\frac{\partial}{\partial t}\nabla\frac{a_\perp^2}{2}\Big|_{\mathbf{laser}} = k_{pe}^2\int_{-\infty}^{\infty}\frac{1}{c}\frac{\partial}{\partial t}\frac{n_b(z)}{n_0}dz\Big|_{\mathbf{beam}}$$

$$\Delta t_{mix}\Big|_{\mathrm{beam-driven}} \propto \frac{\pi}{2\frac{\partial \omega_{pe}(x)}{\partial x}n_b}$$

$$n(x) = n_0\,\frac{x}{L_\Delta}\mathcal{H}(x) \quad \text{and} \quad \omega_{pe}(x) = \omega_{p0}\sqrt{\frac{x}{L_\Delta}}\mathcal{H}(x)$$

$$\Delta t_{mix}\Big|_{\mathrm{beam-driven}} \propto \pi\omega_{p0}^{-1}\sqrt{x}\,\left[\frac{\sqrt{L_\Delta}}{n_b/n_0}\right]$$

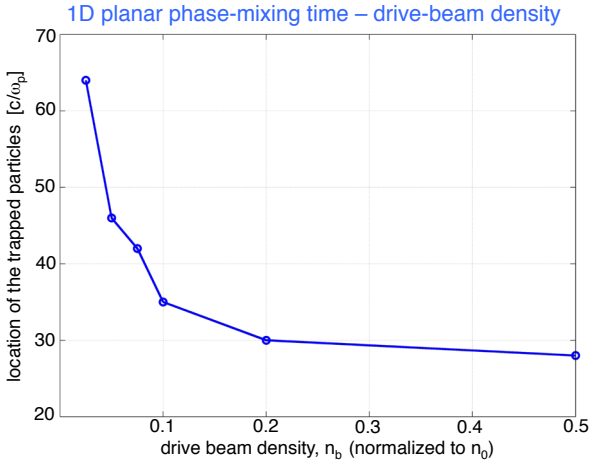

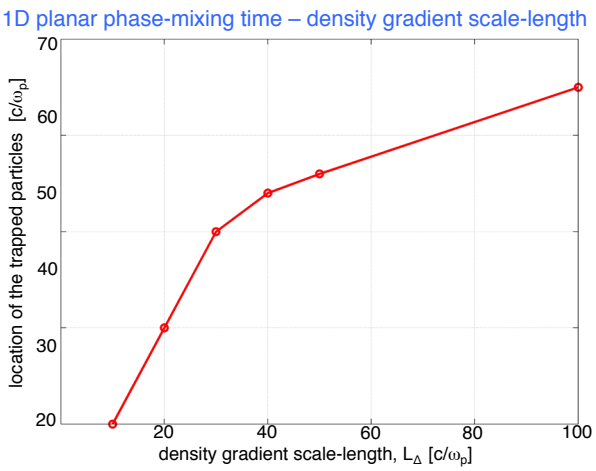

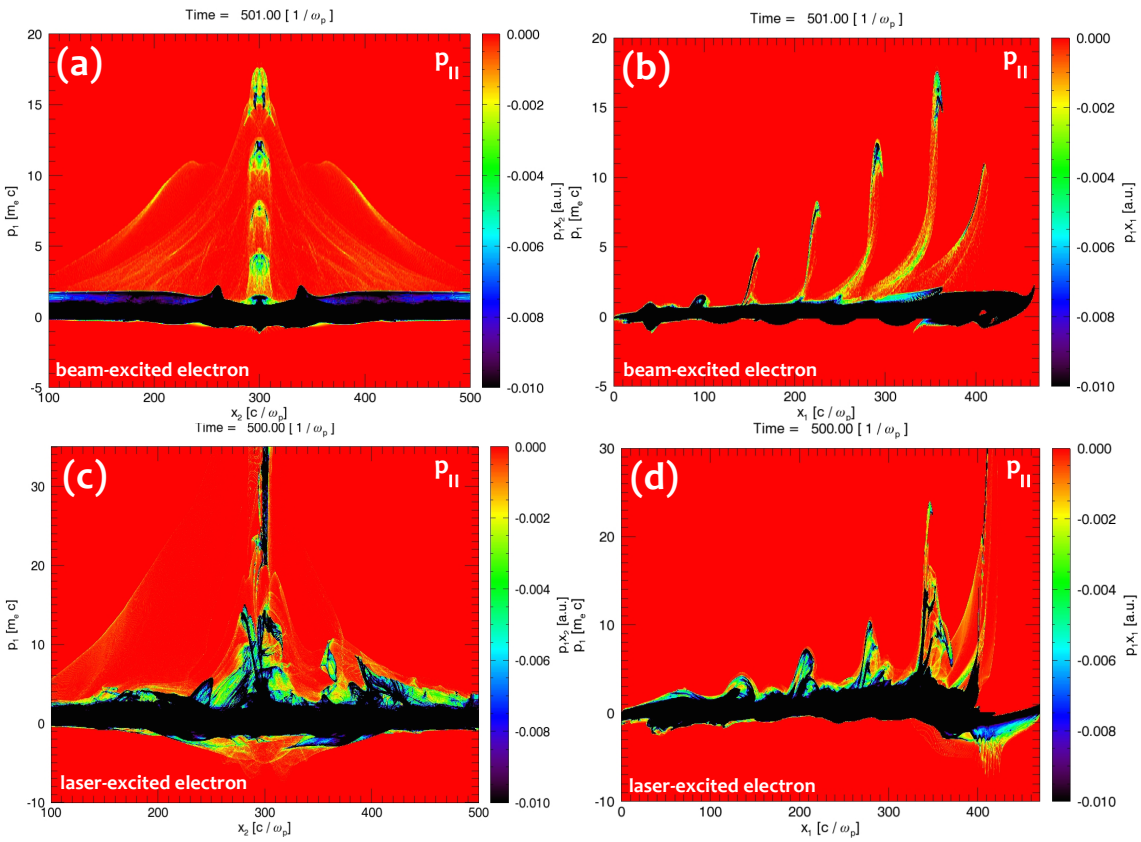

FIGURE 6.10: **The 2D plasma e^- longitudinal momentum phase-space showing trapping of plasma electrons**. Beam-driven phase-spaces are in (a) with transverse dimension (p_1x_2) and (b) with longitudinal (p_1x_1) dimension. Corresponding Laser-driven phase-space are in (c) and (d). The e^- trapped in first laser-driven bucket gain a peak momentum $\gamma_\parallel\beta_\parallel > 30$, whereas in both the beam and laser case, the second bucket e^- only gains, $\gamma_\parallel\beta_\parallel \sim 20$. Also, phase-mixing injection occurs only on the axis.

Self-guiding of a laser pulse by temporal shaping [3] – it is shown that a precursor in the longitudinal shape of a laser pulse helps in self-guiding it for longer, extending the "acceleration length" of the beams which gain a higher energy. We carried out all 2D and 3D proof-of-principle simulations.

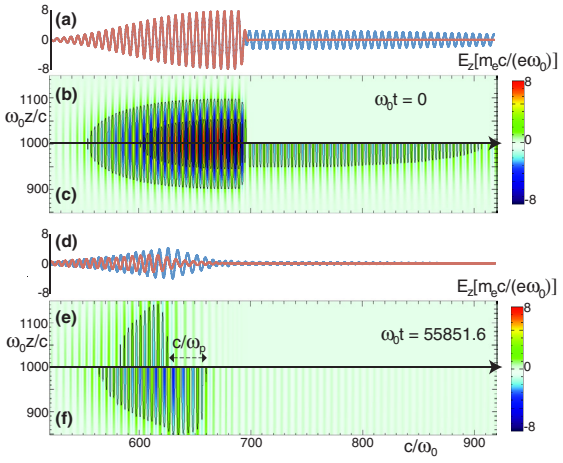

FIG. 1 (color online). 3D PIC simulations demonstrate that a pulse with sharp rise time diffracts while a pulse with tailored profile remains guided. (a) The laser electric field $E_z(x, t = 0)$ for a pulse with sharp rise time (red) and for the precursor of a tailored pulse (blue); the main bodies of the two pulses are identical. The top half of a 2D slice of $E_z(x, y, t = 0)$ for a pulse with sharp rise time is shown in (b) and the bottom half of a slice of $E_z(x, y, t = 0)$ for a tailored pulse in (c). Contours have been drawn for $(e\omega_0 E_z/m_e c) = \pm 1.6, \pm 4.8$. Plots (d), (e), and (f) correspond to (a), (b), and (c) at $\omega_0 t = 55\,951.6$.

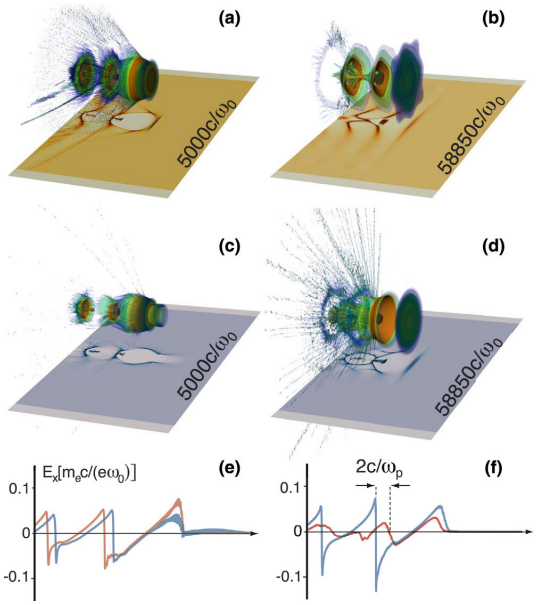

FIG. 2 (color online). Electron density isosurfaces and slices from two 3D PIC simulations, the same as in Fig. 1. In (a) and (b) a pulse with sharp rise time [Fig. 1(b)] is used. In (c) and (d) the pulse has a tailored profile [Fig. 1(c)]. Panels (e) and (f) show the electric field $E_x(x)$ along the laser propagation axis with red (blue) lines for the sharp (tailored) profile.

Figure 6 - Improved self-guiding of a laser pulse with precursor extends the acceleration length resulting in higher electron energy of the trapped electron beam

Stated goal # 2 - Theoretical study of laser-plasma proton acceleration [6][7]

We analytically and computationally analyzed the longitudinal instabilities of the laser-plasma interactions at the critical layer [2]. Specifically, the process of "Doppler-shifted Ponderomotive bunching" is significant to eliminate the very high-energy spread and understand the importance of chirping the laser pulse frequency. We intend to publish the results of the mixing process in 2-D. We intend to publish Chirp-induced transparency.

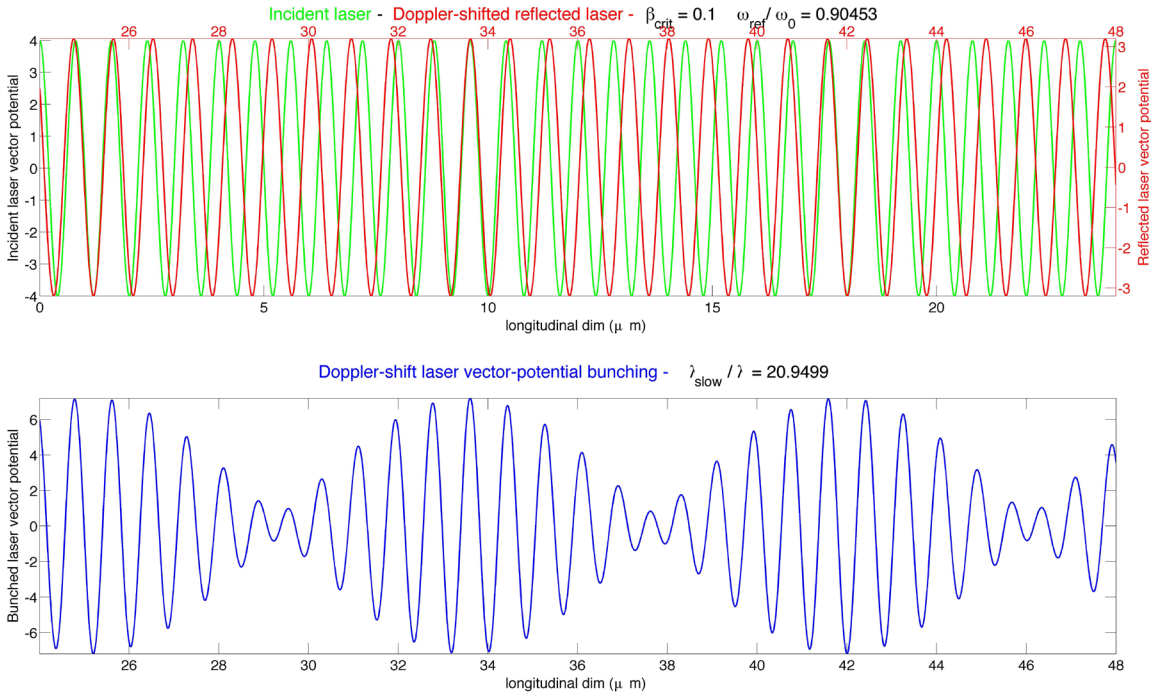

Figure 7 - Mixing of forward (GREEN) and reflected laser pulse (RED) off the critical layer significantly modify the drive pulse (BLUE) by inducing *Doppler-shifted Ponderomotive Bunching* on it

We compared the motion of the plasma critical layer in heavy-ion plasma through relativistically-induced transparency to light-ion plasma through radiation pressure and the results were summarized in [7].

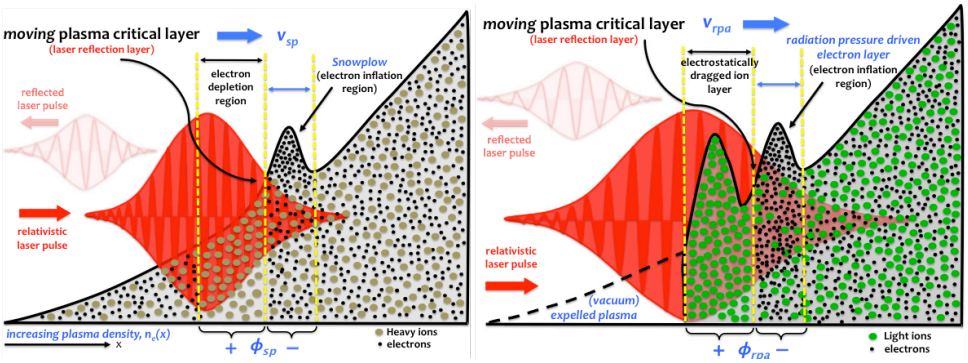

Figure 8 - Schematic to demonstrate the difference between relativistically induced transparency and radiation pressure driven motion